Journal of Hazardous Materials 182 (2010) 386–393

Contents lists available at ScienceDirect

Journal of Hazardous Materials

journal homepage: www.elsevier.com/locate/jhazmat

Synthesis and characterization of thermally stable Sm,N co-doped TiO_2 with highly visible light activity

Yunfei Ma[a], Jinlong Zhang[a,b,*], Baozhu Tian[a], Feng Chen[a], Lingzhi Wang[a]

[a] Key Laboratory for Advanced Materials and Institute of Fine Chemicals, East China University of Science and Technology, 130 Meilong Road, Shanghai 200237, PR China
[b] School of Chemistry and Materials Science, Guizhou Normal University, Guiyang 550001, PR China

ARTICLE INFO

Article history:
Received 1 November 2009
Received in revised form 20 May 2010
Accepted 11 June 2010
Available online 18 June 2010

Keywords:
TiO2
Sm–N co-doping
Photocatalysis
Visible light

ABSTRACT

Samarium and nitrogen co-doped titania (Sm/N-TiO_2) was successfully prepared via coprecipitation method. The resulting materials were characterized by X-ray diffraction (XRD), N_2 physical adsorption, UV–vis absorbance spectroscopy, X-ray photoelectron spectroscopy (XPS), high-resolution transmission electron microscopy (HRTEM) and Fourier transform infrared (FTIR) spectra. Experimental results indicated that samarium doping inhibited the growth of crystalline size and the transformation from anatase to rutile phase. The photocatalytic activities of the samples were evaluated for degradation of salicylic acid under visible light irradiation. It was found that the Sm/N-TiO_2 samples presented much higher photocatalytic activity than N-TiO_2 and pure TiO_2 under visible light irradiation. This could be attributed to the appropriate crystallite size, more efficient separation of electrons and holes on Sm/N-TiO_2. In our experiments, the optimal dopant amount of samarium was 1.5% for the maximum photocatalytic degradation and the sample calcined at 400 °C showed the best reactivity.

1. Introduction

Titanium dioxide (TiO_2) has received a great deal of attention due to its chemical stability, non-toxicity, low cost, and other advantageous properties. It has been employed in self-cleaning, deodorant, anti-bacteria etc, and is expected to be applied to the pollution control to decompose toxic materials in air and waste water [1–4]. However, titania shows photocatalytic activity only under UV light irradiation because of its band gap value of around 3.0 eV for rutile and 3.2 eV for anatase. It is known that the UV part of the solar spectrum only accounts for about 5% of the incoming solar energy. On the other hand, the photocatalytic activity of TiO_2 is limited by fast charge carrier recombination and low interfacial charge-transfer rates of photogenerated carriers [5]. In order to enhance the photocatalytic activity of TiO_2, extending absorption range of TiO_2 into visible light region and suppressing the recombination of excited electrons and holes are two main subjects for the increased utility of TiO_2.

Recently, there are many reports about the modification of TiO_2 by non-metal such as nitrogen. Since Sato [6] reported that the calcination of NH_4Cl or NH_4OH with titanium hydroxide caused the photocatalytic sensitization of TiO_2 into the visible light region, various synthetic routes like calcinations in the presence of nitrogen and ammonia [7,8], sputtering method [9], sol–gel route [10], microemulsion method [11], homogenous precipitation [12] have been widely studied for nitrogen doped TiO_2. Among these methods, sputtering method need expensive and complicated equipment; the sol–gel route and microemulsion method need much organic solvent or need rinse by solvent and high temperature calcination to remove the organic species, which may lead to the growth of the particles. Xu et al. [12] prepared N-TiO_2 photocatalysts with visible light response via a low-temperature precipitation treatment of $TiCl_4$ by ammonia with the presence of glacial acetic acid. In this synthesis route, $TiCl_4$ was used as the inorganic Ti precursor and there was not much organic solvent. The doping of nitrogen has reduced the energy band gap efficiently. In order to separate the excited electrons and holes efficiently, transition metals were used as the dopant. As to the lanthanide ions, for its special 4f electron configurations, the ions are known for their ability to form complexes with various Lewis bases (e.g., acids, amines, aldehydes, alcohols, thiols, etc.) through interaction of these functional groups with the f-orbitals of the lanthanides. Moreover, rare earth can retard the transformation from anatase phase to rutile phase. It is well known that anatase is beneficial to the photocatalysis. Therefore, rare earth doped TiO_2 has attracted researcher's great interest [13–17]. Xu et al. [18] prepared a series of rare earth metal ions doped TiO_2 by sol–gel method. The results showed that rare earth ions doping enhanced the photocatalytic activity of TiO_2. Ranjit et al. [19,20] reported the increase of saturated adsorption capacity and adsorption equilibrium constants simultaneously

* Corresponding author at: Key Laboratory for Advanced Materials and Institute of Fine Chemicals, East China University of Science and Technology, 130 Meilong Road, Shanghai 200237, PR China. Tel.: +86 21 64252062; fax: +86 21 64252062.
E-mail address: jlzhang@ecust.edu.cn (J. Zhang).

0304-3894/$ – see front matter © 2010 Elsevier B.V. All rights reserved.
doi:10.1016/j.jhazmat.2010.06.045

for salicylic acid, trans-cinnamic acid, and *p*-chlorophenoxyacetic acid owing to Eu^{3+}, Pr^{3+}, Yb^{3+} doping. Li et al. [21] reported that the photodegradation of MBT (2-Mercaptobenzothiazole) and its intermediates were enhanced due to the Nd^{3+} doping. Zhang et al. [22,23] prepared nanocrystalline mesoporous titanium dioxide doped with lanthanide. The anatase-to-rutile phase transformation of nanosized TiO_2 was significantly inhibited by lanthanide doping.

So modification of TiO_2 by co-doping with nitrogen and rare earths is an effective method to synthesize the photocatalysts with higher visible light activity. Shen et al. [24] prepared the N-Ce co-doped photocatalyst using the sol–gel method. They pointed out that nitrogen doping destroyed locally the crystal structure, resulting in the response to the visible light. Cerium atoms existed in the state of Ce_2O_3 and were dispersed on the surface of titania, suppressing the recombination of electron–hole pairs and increasing the photoactivity. The cooperative effect of the nitrogen and cerium improved the photocatalytic activity. Huang et al. [25] reported that Sm and nitrogen co-doped TiO_2 catalysts were prepared via the modified sol–gel hydrothermal method using tetrabutyltitanate as the precursor and annealed at 200 °C. However, a lot of solvent such as ethanol was used during the process.

However, there were few reports on the samarium and nitrogen co-doped TiO_2 by precipitation and use the ammonia and titanium sulfate as the precursor of nitrogen and titanium. In this work, Sm^{3+}/N-TiO_2 nanocrystals were successfully synthesized by coprecipitation method through the hydrolysis of titanium sulfate with ammonia. No organic solvent was used in the process. Various amounts of samarium were doped on the N-TiO_2 by the addition of $Sm(NO_3)_3{\cdot}6H_2O$ to the solution of titanium sulfate. The characterization of the photocatalyst was done by XRD, BET, UV–vis absorption spectra, HRTEM and FTIR. The photocatalytic properties were evaluated for the liquid phase decomposition of salicylic acid under visible light irradiation. The excellent photocatalytic activities of Sm/N-TiO_2 as compared to TiO_2 under visible light and the synergistic effect between nitrogen species and samarium element were studied. The influence of samarium ion dosage and calcination temperature on the photoactivity was also investigated.

2. Experimental

2.1. Samples preparation

Titanium sulfate ($Ti(SO_4)_2$, analytical reagent grade) was used as precursor for the preparation of titania. In a typical procedure, 9.0 g $Ti(SO_4)_2$ was dissolved in 36 mL of deionized water, then stirred to ensure complete dissolution. After that, a 35 wt.% solution of ammonia was added dropwise with vigorous stirring until pH 8.0. After aging in the mother liquid for 12 h, the precipitate obtained was suction-filtered and washed with distilled water until free of sulfate ions (as was confirmed by the $BaCl_2$ test). The N-TiO_2 was finally obtained after the as-prepared filter residue was dried in vacuum at 333 K for 12 h and calcinated at 673 K in air for 2 h. The Sm doped N-TiO_2 was prepared in the presence of certain amount $Sm(NO_3)_3{\cdot}6H_2O$ in the deionized water before adding titanium sulfate. The nominal content of Sm in the samples was 0%, 0.5%, 1.0%, 1.5%, 2.0%, 2.5%, designated as N–TiO_2, 0.5Sm/N–TiO_2, 1.0Sm/N–TiO_2, 1.5Sm/N–TiO_2, 2.0Sm/N–TiO_2, 2.5Sm/N-TiO_2, respectively. The pure TiO_2 was prepared by precipitation the solution of titanium sulfate with sodium hydroxide solution and the rest of the procedure was not changed.

2.2. Characterizations

X-ray diffraction (XRD) patterns of all samples were collected in the range 20–70° with a stepwidth of 0.02° s^{-1} using a Rigaku D/MAX 2550 VB/PC apparatus (Cu Kα radiation, λ = 1.5406 Å), operated at 40 kV and 100 mA. The Brunauer–Emmett–Teller(BET) surface area of the samples were determined through nitrogen adsorption at 77 K (Micromeritics ASAP 2010). All the samples were degassed at 473 K for 2 h before the measurement. The surface morphologies and particle sizes were observed by transmission electron microscopy (TEM, JEM-2011), using an accelerating voltage of 200 kV. The samples were prepared by grinding and subsequent dispersing the powder in acetone and applying a drop of very dilute suspension on carbon-coated grids. The UV–vis absorbance spectra were obtained for the dry-pressed disk samples using a Scan UV–vis spectrophotometer (Varian, Cary500) equipped with an integrating sphere assembly, using $BaSO_4$ as the reflectance sample. The spectra were recorded at room temperature in air within the range 200–800 nm. To investigate the chemical states of the photocatalyst, X-ray photoelectron spectroscopy (XPS) was recorded with PerkinElmer PHI 5000C ESCA System with Al Kα radiation operated at 250 W. The shift of the binding energy due to relative surface charging was corrected using the C 1s as an internal standard at 284.6 eV. Fourier transform infrared (FTIR) spectra were recorded with KBr disks containing the powder sample with the FTIR spectrometer (Nicolet Magna 550).

2.3. Evaluation of photocatalytic activity

The photocatalytic activity was evaluated by measuring the decomposition of 50 mg/L salicylic acid solution. A 1000 W tungsten halogen lamp was used as the light source, surrounded with a water circulation facility at the outer wall through a quartz jacket. The short wavelength components (λ < 420 nm) of the light were cut off using UV cut-off filters. The distance between the lamp and the center of the quartz tube was 10 cm. For a typical photocatalytic experiment, 0.05 g of catalyst powder was added to 50 mL of the above salicylic acid solution in the quartz tube. The initial pH value of the solution was kept at 3.5. Prior to irradiation, the suspensions were magnetically stirred in the dark for 30 min to ensure the establishment of an adsorption/desorption equilibrium. The above suspensions were kept under air-equilibrated conditions before and during the irradiation. After specific intervals, about 4 mL liquid was taken and centrifuged. The supernatant liquid was analyzed by recording the absorbance at 297 nm of salicylic acid solution using a UV–vis spectrophotometer (Varian Cary 100). According to the standard curve of concentration and absorption, the value of $\Delta C/C_0$ was calculated and indicated the decomposition efficiency.

3. Results and discussion

3.1. XRD and BET analysis

XRD patterns of Sm/N-TiO_2 samples with various samarium content and pure TiO_2 calcined at 400 °C for 2 h are presented in Fig. 1. Only the diffraction peaks of anatase TiO_2 can be observed for all samples. With respect to Sm/N-TiO_2 samples, the peak at 25.5° corresponding to characteristic peak of crystal plane (1 0 1) of anatase became broader and the relative intensity decreased with increasing samarium ion dosage. This indicated that samarium ion doping inhibited the phase transformation from amorphous to anatase in the solid. From the (1 0 1) peak of anatase TiO_2, the average size of crystallite was calculated using the Scherrer equation:

$$D = \frac{K\lambda}{\beta \cos\theta}$$

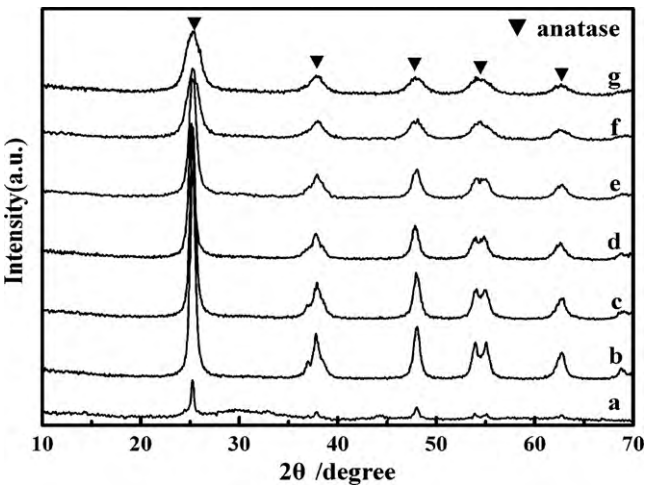

Fig. 1. XRD patterns of different samples calcined at 400 °C (a) pure TiO_2, (b) N-TiO_2, (c) 0.5Sm/N-TiO_2, (d) 1.0Sm/N-TiO_2, (e) 1.5Sm/N-TiO_2, (f) 2.0Sm/N-TiO_2, and (g) 2.5Sm/N-TiO_2.

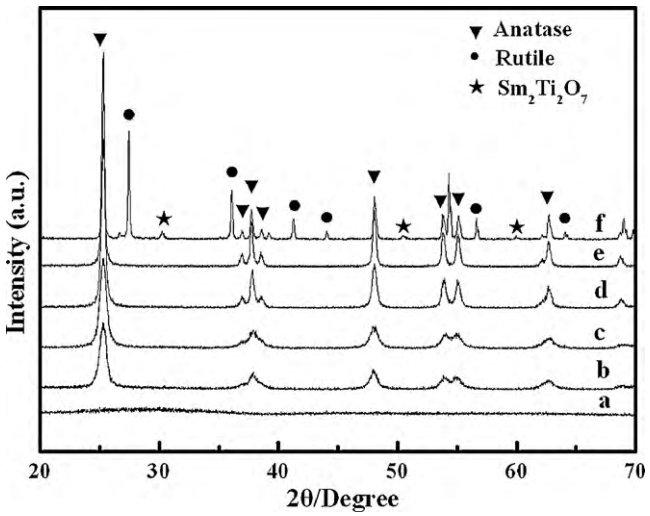

Fig. 2. XRD patterns of 1.5Sm/N-TiO_2 calcined at different temperatures: (a) 300 °C, (b) 400 °C, (c) 500 °C, (d) 600 °C, (e) 800 °C, and (f) 900 °C.

where β is the full width half maximum (FWHM) of the 2θ peak, K is the shape factor of the particles (it equals to 0.89), θ and λ are the incident of angle and the wavelength of the X-rays, respectively. The crystallite size of all samples was shown in Table 1. Compared to pure TiO_2 and N-TiO_2, with the increasing the concentration of Sm, the crystallite size decreased. The N/TiO_2 sample doping with 2.5% samarium only has a crystallite size of 4.8 nm. This reduction in crystallite size is proposed to be due to segregation of the samarium cations at the grain boundary, which inhibited the grain growth by restricting direct contact of grains [26].

The Brunauer–Emmett–Teller(BET) specific surface areas of the TiO_2, N-TiO_2 and Sm/N-TiO_2 samples are also listed in Table 1. The pure TiO_2 has only a specific surface area of 11 m^2/g and the N-TiO_2 has a specific surface area of 58 m^2/g. The surface area of 0.5Sm/N-TiO_2, 1.0Sm/N-TiO_2, 1.5Sm/N-TiO_2, 2.0Sm/N-TiO_2 and 2.5Sm/N-TiO_2 samples are 80, 106, 170, 150, 130 m^2/g, respectively. With the increase of the amount of Sm, the surface area increase from 58 to 170 m^2/g. This is in accordance with the crystallite size. When the amount of samarium exceeds 1.5%, the surface area begins to decrease. The slight reduction in the BET surface area is probably due to the blockage of some of the TiO_2 pores by higher Sm loading. It can be concluded that the deposition of samarium could change the texture properties greatly.

Since the addition of samarium has great effect on the crystallite size when they were calcined at 400 °C, the samples doped with 1.5 mol% samarium calcined at different temperature were investigated. Fig. 2 shows the XRD patterns of the samples calcined from 300 to 900 °C. It is reported that the transformation of titania from anatase to rutile for TiO_2 will occur at 600 °C. But when samarium was doped in the N-TiO_2, the 1.5Sm/N-TiO_2 remains only anatase phase even the annealing temperature are up to 800 °C. However, rutile phase appeared when the calcination temperature reached 900 °C. The retardation of phase transformation may be due to the stabilization of the anatase phase by the surrounding rare earth ions via the formation of Ti–O–Sm element bonds [27]. Additionally, another new phase was also observed which is attributed to samarium titanium oxide ($Sm_2Ti_2O_7$) [JCPDS no. 16-0400]. It can be speculated that the suppression of phase transformation may be due to the presence of Sm_2O_3 around the TiO_2 nanoparticles. When the temperature was above 900 °C, most Sm_2O_3 may react with TiO_2 at the interface to form $Sm_2Ti_2O_7$, there was few Sm_2O_3 around the TiO_2 to prevent the nucleation; thus rutile phase formed.

Table 1
The characteristics of N-TiO_2 containing different samarium content calcined at 400 °C.

Sample	Crystallite size D(1 0 1)/(nm)	Specific surface area (m^2/g)
Pure TiO_2	21	11
N-TiO_2	16.5	58
(0.5%)Sm/N-TiO_2	14.1	80
(1.0%)Sm/N-TiO_2	11.3	106
(1.5%)Sm/N-TiO_2	8.8	170
(2.0%) Sm/N-TiO_2	5.8	150
(2.5%)Sm/N-TiO_2	4.8	130

The XRD patterns of the samples doped with different amounts of Sm calcined at 900 °C are shown as Fig. 3. The ratio of anatase to rutile in the sample was calculated by employing the well-known formula [28]:

$$X_A = \left[1 + 1.265\left(\frac{I_R}{I_A}\right)\right]^{-1}$$

where X_A is the fraction of anatase in the mixture, and I_A is the (1 0 1) peak intensity of anatase, I_R is the (1 1 0) peak intensity of rutile, and 1.265 is the scattering coefficient. The results were listed

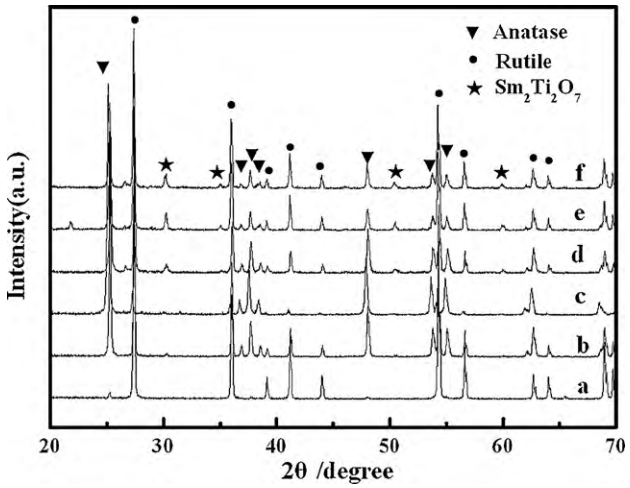

Fig. 3. XRD patterns of different samples calcined at 900 °C (a) N-TiO_2, (b) 0.5Sm/N-TiO_2, (c) 1.0Sm/N-TiO_2, (d) 1.5Sm/N-TiO_2, (e) 2.0Sm/N-TiO_2, and (f) 2.5Sm/N-TiO_2.

Table 2
The ratio of anatase and rutile of titania doped with different amount of Sm calcined at 900 °C.

Sample	Anatase %	Rutile %
N-TiO_2	2	98
(0.5%)Sm/N-TiO_2	51	49
(1.0%)Sm/N-TiO_2	90	10
(1.5%)Sm/N-TiO_2	54	46
(2.0%) Sm/N-TiO_2	34	66
(2.5%)Sm/N-TiO_2	31	69

in Table 2. It can be found that with the increase of samarium, the ratio of anatase increase, when the amount of samarium was up to 1%, the anatase phase reached the maximum; then further increase of samarium led to decrease anatase phase. Other researchers also found the similar results [22]. At the same time, when the amount of samarium exceeded 1%, the new phase of $Sm_2Ti_2O_7$ appeared. With the increase of Sm, the corresponding intensity of this peak increased. This further supported the above result that the formation of $Sm_2Ti_2O_7$ reduced the amount of Sm_2O_3 surrounding TiO_2, so anatase phase began to transform to rutile phase.

3.2. TEM analysis

The TEM images of N-TiO_2 and 1.5Sm/N-TiO_2 nanoparticles calcined at 400 °C are shown as Fig. 4(a and b). The N-TiO_2 nanoparticles have irregular morphology and the diameter is more than 15 nm. 1.5Sm/N-TiO_2 sample has uniform morphology with an average diameter of 8 nm or so, which are in good agreement with the XRD evaluation. Fig. 4(c and d) shows part of one nanocrystal having several lattice planes with perfect crystallinity. The lattice fringes are characteristics of the anatase TiO_2 crystal, in which the *d*-spacing of 0.352 nm corresponds to the distance between the (1 0 1) planes.

3.3. UV–vis absorbance spectra

The UV–vis absorbance spectra of samples with different amount of Sm loading are shown as Fig. 5A. It can be seen that the N-TiO_2 sample presents a significant absorption in the visible region between 400 and 550 nm, which is the typical absorption feature of nitrogen doped TiO_2. Kubelka–Munk function was used to estimate the band gap energy of the prepared samples by plotting $(\alpha hv)^{1/2}$ versus energy of light(see Fig. 5B). Results indicated that the band gap energies of pure TiO_2 and N-TiO_2 was 3.09 and 2.84 eV, respectively. With the doping of samarium, the weak blue shift is observed in the Sm/N-TiO_2 and the band gap energy of 1.5Sm/N-TiO_2 is 2.89 eV. This phenomenon can be ascribed to the quantum size effect, because the addition of Sm has greatly decreased the crystal size of TiO_2. Moreover, the band gap of Sm_2O_3 is about 3.6 eV [29], the high dispersed lanthanide oxide on the surface of TiO_2 reduce the absorption in the visible region.

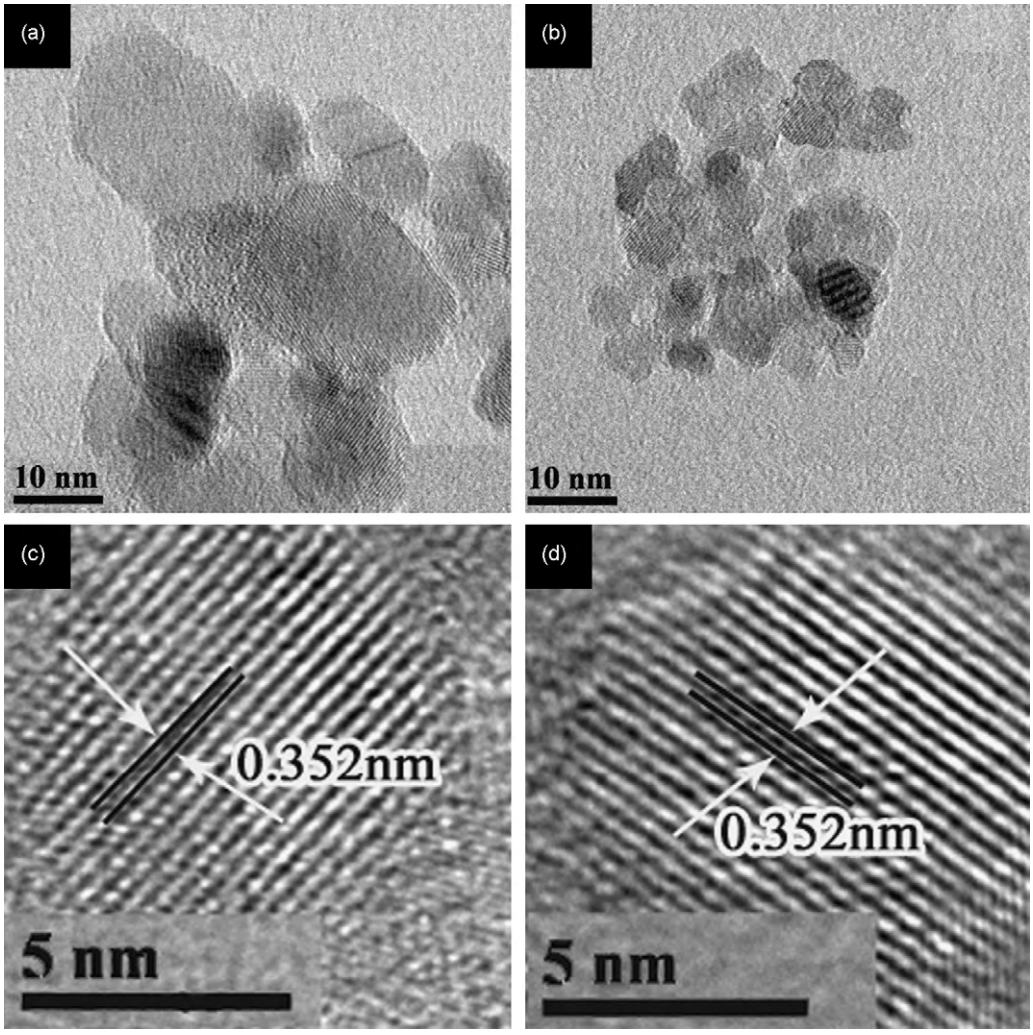

Fig. 4. HRTEM of N-TiO_2 and 2.5%Sm/N-TiO_2.

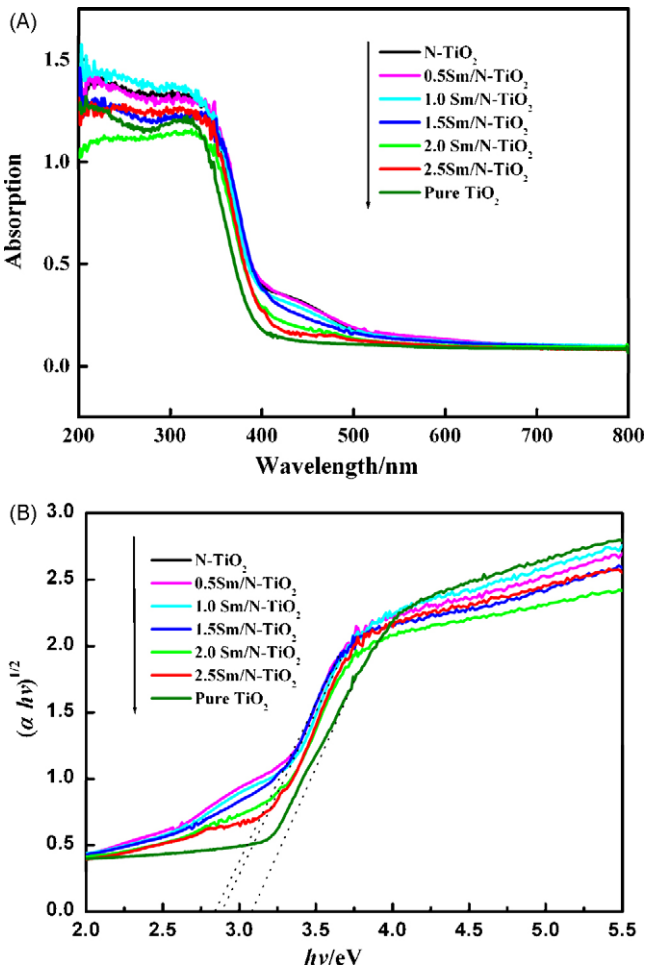

Fig. 5. UV–vis absorption spectra of pure TiO_2, N-TiO_2 and (*x*)Sm/N-TiO_2.

3.4. XPS analysis

The XPS spectra of 1.5Sm/N-TiO_2 calcined at 400 °C are shown as Fig. 6. Fig. 6(a) shows the N 1s XPS spectrum. It can be seen that there is a broad peak from 396 to 403 eV, which is typical nitrogen-doped titanium dioxide [8,30,31]. After fitting of the curve data, two peaks are obtained at 400.0 eV (peak 1) and 397.6 eV(peak 2). The first peak is attributed to the anionic N- in Ti–O–N, that is the interstitial N. The second peak is assigned to the substitutional N in O–Ti–N linkages, which may be related to the active sites of the photocatalysis [8]. The binding energy of second peak is higher than that of TiN appearing at 397.2 eV [32], which may be due to higher electron negativity of oxygen than nitrogen, so the electron density on the nitrogen decrease and binding energy increase. This is also further supported by the results of XPS spectrum for the Ti 2p region as shown in Fig. 6b. The $Ti2p_{3/2}$ core levels of the N-TiO_2 is 458.4 eV, according to other literature and XPS handbook, pure TiO_2 appears at 459.05 eV. The binding energy of $Ti2p_{3/2}$ after nitrogen doping decreases and suggests different electronic interactions of Ti with anions, which causes partial electron transfer from the N to the Ti and an increase in the electron density of Ti because of the lower electron negativity of nitrogen compared to oxygen. This further verified that nitrogen was incorporated into the lattice and substituted for oxygen.

The XPS of O 1s are shown in Fig. 6c. The peak at 529.9 eV is the characteristic peak of Ti–O bond. An additional peak for N-TiO_2 appears at about 532.0 eV and previously was attributed to the presence of the hydroxyl O atoms. Fig. 6d shows the XPS spectrum of Sm 3d. The curve can be fitted into two peaks. The peak at 1084.3 eV is corresponding to the bond of Sm–O. The peak at 1082.2 eV is corresponding to the bond of Sm–O–Ti. Although the ionic radius of Sm^{3+}(1.08 Å) is bigger than the ionic radius of Ti^{4+}(0.68 Å) and the Sm^{3+} ions can't enter into the lattice of TiO_2, Ti^{4+} ion may enter into the lattice of the Sm_2O_3 which could cause the change of electron field of Sm^{3+} and increase the electron density, and hence decrease the binding energy of Sm^{3+}.

Table 3
The first-order kinetic constants (k, min^{-1}) and relative coefficient(R^2) for degradation of salicylic acid under visible light irradiation.

Photocatalysts	K (min^{-1})	R^2	Degradation %
Pure TiO_2	0.0001	0.9930	3.5
N-TiO_2	0.0015	0.9951	34.6
0.5Sm-N/TiO_2	0.0023	0.9985	49.8
1.0Sm-N/TiO_2	0.0031	0.9958	60.4
1.5Sm-N/TiO_2	0.0037	0.9956	66.9
2.0Sm-N/TiO_2	0.0029	0.9959	57.5
2.5Sm-N/TiO_2	0.0026	0.9927	53.7

3.5. Photocatalytic activity

3.5.1. Effect of activation temperature

The photocatalytic activities of 1.5Sm/N-TiO_2 calcined at different temperature from 300 to 600 °C are shown as Fig. 7. When the calcination temperature was 300 °C, the main phase was amorphorous. The degradation of salicylic acid was only 20%. With the increase of the calcination temperature, the crystallinity of the samples became more and more better, and the grain size increased from 8.8 nm calcined at 400 °C to 17.8 nm calcined at 600 °C. Accordingly, the degradation decreased from 68% to 27%. Therefore it was concluded that 400 °C was the optimal calcination temperature for the best photoactivity because of the appropriate particle size and high surface area. Furthermore, the calcination temperature has a great influence on the optical absorption. The color of the sample calcined at 400 °C was yellow. When the sample was calcined at 500 and 600 °C, the color of the samples became pale. The nitrogen species in the lattice may be removed. Wang et al. [33] reported that the decrease of absorption in visible light region is attributed to the loss of nitrogen in TiO_2 during the calcination process. It will become much easier for nitrogen to be replaced by oxygen in the air under high temperature. Sathish et al. [34] also reported the similar phenomenon. It can be concluded that sample calcined under 400 °C can degrade the salicylic acid efficiently for the existence of nitrogen species in the lattice.

3.5.2. Effect of nitrogen and samarium

The photocatalytic degradation of salicylic acid under visible light irradiation over Sm, N co-doped TiO_2 samples calcined at 400 °C were evaluated and the results are shown in Fig. 8. It is obvious that the samarium doped N-TiO_2 have higher activity than the pure TiO_2. A better and more quantitative method of presenting the activities of a series of samarium-doped N-TiO_2 photocatalysts is the use of the rate constant k, where k is calculated according to the following equation:

$$\ln \frac{C_0}{C_t} = kt$$

where C_0 and C_t represent initial equilibrium concentration and the reaction concentration of salicylic acid, respectively. In photocatalytic reactions, k is almost independent of temperature and concentration because of the photoactivtion process depends only on the radiant flux and on the visible light spectrum of the lamp. The rate constants were listed in Table 3. The rate constant k of pure TiO_2 and N-TiO_2 is 0.0001 and 0.0015 min^{-1} with the

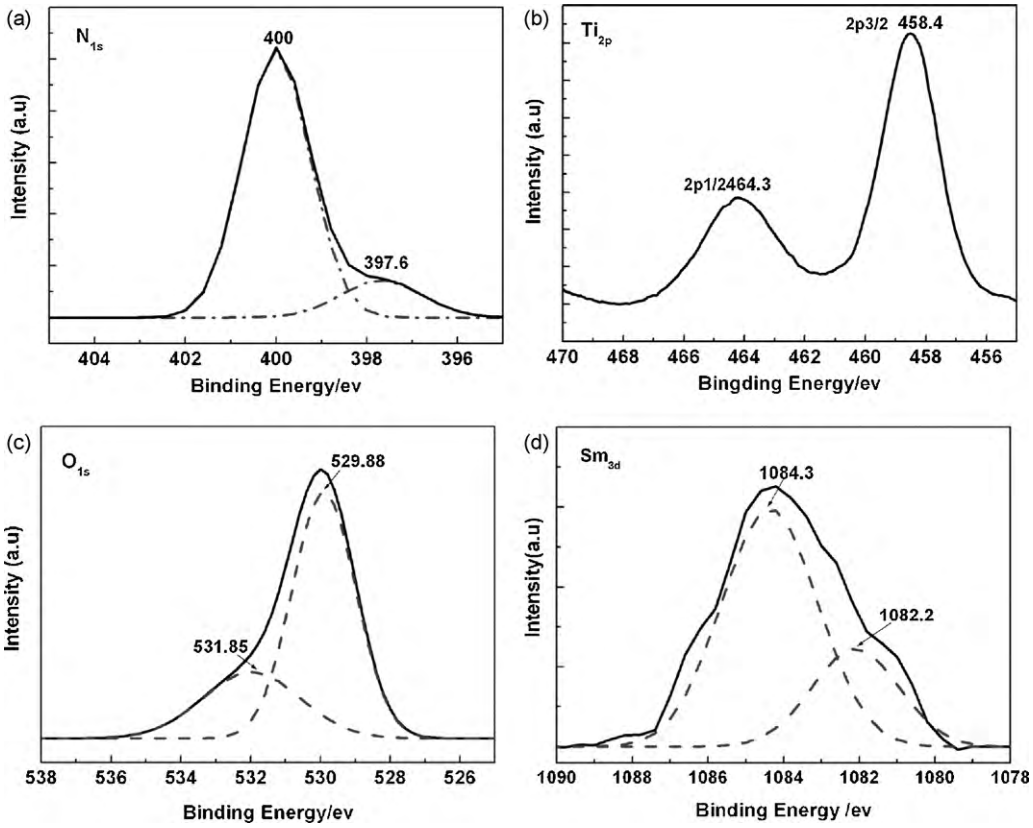

Fig. 6. XPS spectra of N 1s, Ti 2p, O 1s, and Sm 3d for 1.5Sm/N-TiO_2 sample.

degradation of 3.5% and 35%, respectively. The doping of nitrogen into the TiO_2 has enhanced the degradation of salicylic acid for the absorption in the visible light. With the increase of the Sm^{3+} dosage, the photocatalytic activity increased initially, then decreased when Sm^{3+} doping content was over an optimal dosage. Obviously, 1.5Sm/N-TiO_2 achieved the best photocatalytic performance with k of 0.0037 min^{-1} and the highest degradation of 67%. The optimum samarium-doped amount was 1.5 mol% in this experiment, which might be due to the fact that there was an optimum doping content in TiO_2 particles for the most efficient separation of photoinduced electron-hole pairs. Xu et al. [18] find the concentration of dopant ions is related with the space charge region. Only when the thickness of space charge region is equal to the light penetration depth, the electron–hole pairs can be efficiently separated. In our experiment, 1.5 mol% dosage is the optimal amount for the separation of the carriers.

To interpret the enhanced photocatalytic activity of the modified TiO_2, a set of adsorption experiments were carried out to evaluate the extent of saturated adsorption. The saturated adsorption of salicylic acid was shown in Fig. 9. With the increase of the samarium dopants, the saturated adsorption amount of salicylic acid increased. Our results are in agreement with those reported by Liang et al. [35]. The adsorption amount of salicylic acid on

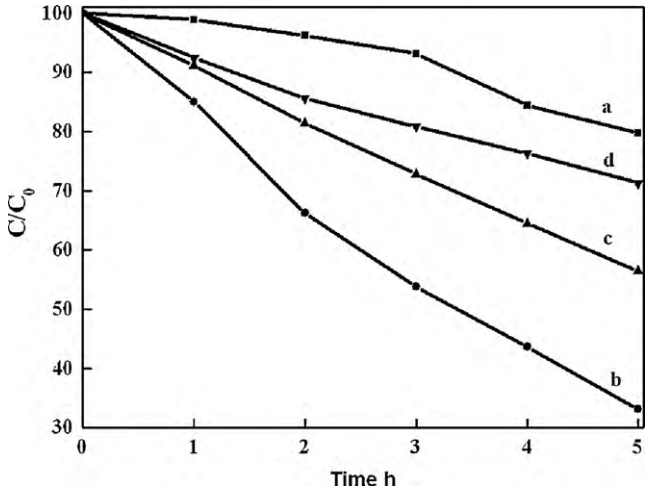

Fig. 7. Photocatalytic degradation of salicylic acid using 1.5Sm/N-TiO_2 calcined at different temperature: (a) 300 °C, (b) 400 °C, (c) 500 °C, and (d) 600 °C.

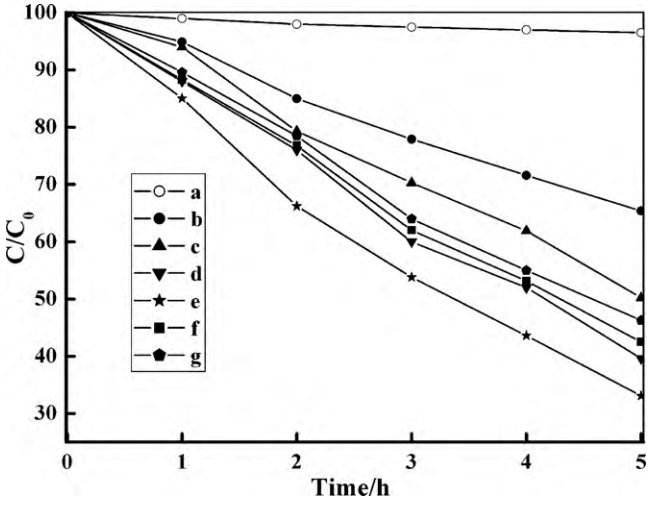

Fig. 8. Photocatalytic degradation of salicylic acid using different samples (a) pure TiO_2, (b) N-TiO_2, (c) 0.5Sm/N-TiO_2, (d) 1.0Sm/N-TiO_2, (e) 1.5Sm/N-TiO_2, (f) 2.0Sm/N-TiO_2, and (g) 2.5Sm/N-TiO_2.

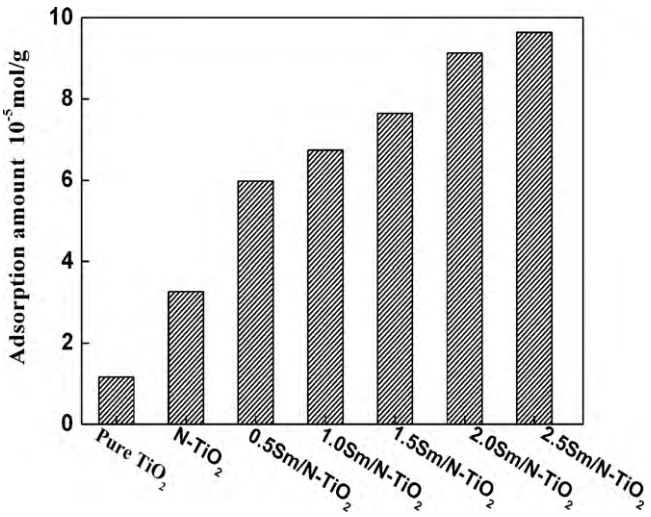

Fig. 9. The saturated adsorption amount of salicylic acid on pure TiO_2 and (x)Sm/N-TiO_2 calcined at 400 °C.

the 1.5Sm/N-TiO_2 was found to be five times higher than that of pure TiO_2. This indicated that the doping of samarium is beneficial to the adsorption of salicylic acid. Ranjit et al. [19] reported that the lanthanide oxide doped TiO_2 catalysts changed bright yellow upon immersion in salicylic acid solutions, whereas the pure TiO_2 changed pale yellow. The enhanced adsorption amount is attributed to the formation of Lewis acid–base complexes between the samarium ions in the modified TiO_2 and salicylic acid. This phenomenon was also observed in our experiments. Additionally, the FTIR of the samples after adsorption experiment were represented in Fig. 10. No obvious signal of salicylic acid was observed in Fig. 10(a and b). But the absorption band at 1600, 1240 cm^{-1} corresponding to C–C and C–O stretch vibration, respectively of salicylic acid appeared on the sample of 1.5Sm/N-TiO_2 after adsorption experiment. However the peak between 1690 and 1730 cm^{-1} corresponding to $\upsilon_{C=O}$ stretching vibration disappeared. The new peaks corresponding to 1385 and 1554 cm^{-1} are the symmetrical vibration and asymmetrical vibration of carboxyl [36]. The results of infrared spectra indicated that the rare earth ions coordinated with salicylic acid. It can be induced that the dopant samarium is the main active site for the adsorption of salicylic acid.

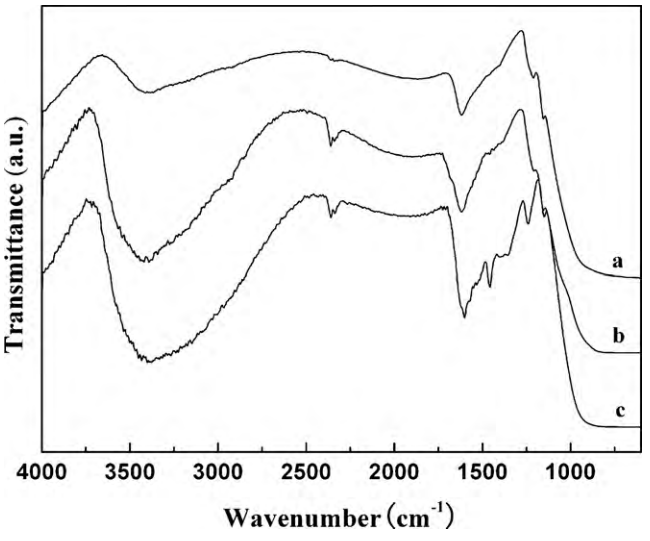

Fig. 10. FTIR spectra of samples after adsorption experiment (a) pure TiO_2, (b) N-TiO_2, and (c) 1.5Sm/N-TiO_2.

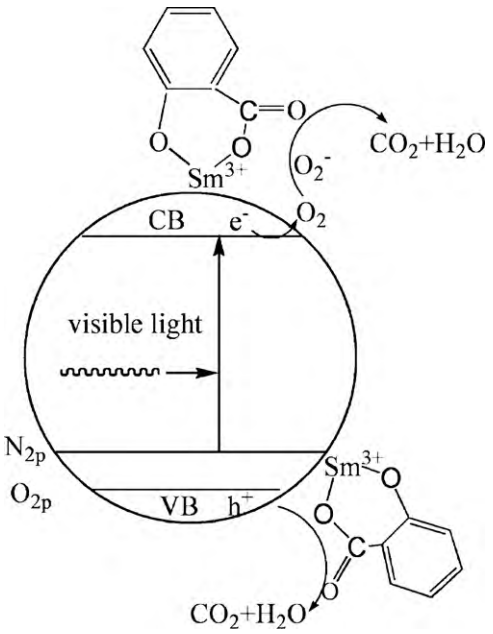

Scheme 1. Photocatalysis process of Sm/N-TiO_2 photocatalyst under visible light irradiation.

It is well known that the photocatalytic activity is related with the adsorption of salicylic acid and the improvement of the interfacial charge transfer reaction. Interfacial charge transfer is possible only when the donor or acceptor is pre-adsorbed before the photocatalytic reaction. From Fig. 9, we can see that all modified catalysts show stronger adsorption capacities than pure TiO_2. So it is positive for some samarium deposited on the N-TiO_2 which is beneficial for the adsorption of salicylic acid and the interfacial charge transfer. When the dosage of samarium exceeded 1.5%, although the adsorption of salicylic acid increased, the photoactivity decreased. Excess amount of samarium oxide dispersed on the surface of TiO_2 would become the recombination center of the electron–hole pairs and result in low photoactivity.

Furthermore, from Table 1, we can see the crystallite size of the 1.5Sm/N-TiO_2 is 8.8 nm. When the dopant is less than 1.5%, the crystallite size is bigger than 8.8 nm and the specific surface area is small. When the dopant is more than 1.5%, the crystallite size is as small as 5 nm or so, the specific surface area decrease for the blockage of the excess samarium on the surface. Additionally, the quantum effect results in the absorption region shift to the blue region decreasing the absorption in the visible light. Therefore, 1.5Sm/N-TiO_2 has the appropriate crystallite size and the highest surface area, which will lead to has more active sites. Accordingly, 1.5Sm/N-TiO_2 exhibits the best photocatalytic performance. The whole photocatalysis process can be described as Scheme 1. On the one hand, the N 2p energy level situated above the valence band (as shown in Scheme 1) and it will form a narrower band gap than that of pure TiO_2. This extended the absorption into the visible light region. Under the visible light irradiation, photons from visible irradiation were utilized to generate electrons and holes. The electrons were excited from the N impurity level to the conduction band, the O_2 adsorbed on the surface captured the electrons to form O_2^-, which will react with the organic materials. The holes can react with chemisorbed OH^- or H_2O to produce hydroxyl radicals ($OH^\bullet$) which have strong capable of oxidizing and destroying organic molecules in aqueous media. According to the adsorption experiment results and characterization of the sample after adsorption, the salicylic acid was pre-adsorbed on the surface of Sm/N-TiO_2 for the interaction of salicylic acid with the 4f orbitals of samarium. The sample of Sm/N-TiO_2 concentrated the salicylic acid on the surface by Sm

coordinated with salicylic acid. It is easier for $OH^{\bullet}$ and O_2^- react with salicylic acid on the surface of TiO_2 than in aqueous media. The synergistic effects of samarium and nitrogen led to high photodegradation of salicylic acid under visible light irradiation.

4. Conclusion

High visible light induced photocatalyst of Sm/N-TiO_2 was successfully prepared by coprecipitation method. Nitrogen doping extended the absorption to visible light region. The samarium doping inhibited the anatase-to-rutile phase transformation and retarded the growth of crystallite. When the calcination temperature was as high as 900 °C, the anatase phase began to transform to rutile phase. The highest enhancement in photocatalytic activity was obtained with 1.5 mol% samarium doping and calcined at 400 °C. This high activity was attributed to the appropriate crystallite size, high surface area, good adsorptive capacity, efficient inhibition of the recombination of the electrons and holes by the samarium, and the synergic action between samarium and nitrogen.

Acknowledgment

This work was supported by National Nature Science Foundation of China (20773039 and 20977030), National Basic Research Program of China (973 Program, 2007CB613301 and 2010CB732306), Science and Technology Commission of Shanghai Municipality (10520709900) and the Fundamental Research Funds for the Central Universities.

References

[1] A.L. Linsebigler, G. Lu, J.T. Yates, Photocatalysis on TiO_2 surfaces: Principles, mechanisms, and selected results, Chem. Rev. 95 (1995) 735–758.
[2] M.R. Hoffmann, S.T. Martin, W. Choi, D.W. Bahnemann, Environmental applications of semiconductor photocatalysis, Chem. Rev. 95 (1995) 69–96.
[3] T. Minabe, D.A. Tryk, P. Sawunyama, Y. Kikuchi, K. Hashimoto, A. Fujishima, TiO_2-mediated photodegradation of liquid and solid organic compounds, J. Photochem. Photobiol. A: Chem. 137 (2000) 53–62.
[4] A. Fujishima, T.N. Rao, D.A. Tryk, Titanium dioxide photocatalysis, J. Photochem. Photobiol. C 1 (2000) 1–21.
[5] A. Kumar, A.K. Jain, Photophysics and photocatalytic properties of Ag^+-activated sandwich Q–CdS–TiO_2, J. Photochem. Photobiol. A: Chem. 156 (2003) 207–218.
[6] S. Sato, Photocatalytic activity of NO_x-doped TiO_2 in the visible light region, Chem. Phys. Lett. 123 (1986) 126–128.
[7] H. Irie, Y. Watanabe, K. Hashimoto, Nitrogen-concentration dependence on photocatalytic activity of $TiO_{2-x}N_x$ powders, J. Phys. Chem. B 107 (2003) 5483–5486.
[8] R. Asahi, T. Morikawa, T. Ohwaki, K. Aoki, Y. Taga, Visible-light photocatalysis in nitrogen-doped titanium oxides, Science 293 (2001) 269–271.
[9] T. Lindgren, J.M. Mwabora, E. Avendano, J. Jonsson, A. Hoel, C.-G. Granqvist, S.-E. Lindquist, Photoelectrochemical and optical properties of nitrogen doped titanium dioxide films prepared by reactive dc magnetron sputtering, J. Phys. Chem. B 107 (2003) 5709–5716.
[10] D.G. Huang, S.J. Liao, J.M. Liu, Z. Dang, L. Petrik, Preparation of visible-light responsive N-F-codoped TiO_2 photocatalyst by a sol–gel solvothermal method, J. Photochem. Photobiol. A: Chem. 184 (2006) 282–288.
[11] Y. Cong, J.L. Zhang, F. Chen, M. Anpo, Synthesis and characterization of nitrogen-doped TiO_2 nanophotocatalyst with high visible light activity, J. Phys. Chem. C. 111 (2007) 6976–6982.
[12] J.H. Xu, W.L. Dai, J. Li, Y. Cao, H. Li, H. He, K. Fan, Simple fabrication of thermally stable apertured N-doped TiO_2 microtubes as a highly efficient photocatalyst under visible light irradiation, Catal. Commun. 9 (2008) 146–152.
[13] J.W. Shi, J.t. Zheng, P. Wu, Preparation, characterization and photocatalytic activities of holmium-doped titanium dioxide nanoparticles, J. Hazard. Mater. 161 (2009) 416–422.
[14] C.P. Sibu, S.R. Kumar, P. Mukundan, K.G.K. Warrier, Structural modifications and associated properties of lanthanum oxide doped sol–gel nanosized titanium oxide, Chem. Mater. 14 (2002) 2876–2881.
[15] K.M. Parida, N. Sahu, Visible light induced photocatalytic activity of rare earth titania nanocomposites, J. Mol. Catal. A: Chem. 287 (2008) 151–158.
[16] K.V. Baiju, C.P. Sibu, K. Rajesh, P.K. Pillai, P. Mukundan, K.G.K. Warrier, W. Wunderlich, An aqueous sol–gel route to synthesize nanosized lanthana-doped titania having an increased anatase phase stability for photocatalytic application, Mater. Chem. Phys. 90 (2005) 123–127.
[17] J. Zhou, Y. Zhang, X.S. Zhao, A.K. Ray, Photodegradation of benzoic acid over metal-doped TiO_2, Ind. Eng. Chem. Res. 45 (2006) 3503–3511.
[18] A.W. Xu, Y. Gao, H.Q. Liu, The preparation, characterization, and their photocatalytic activities of rare-earth-doped TiO_2 nanoparticles, J. Catal. 207 (2002) 151–157.
[19] K.T. Ranjit, I. Willner, S.H. Bossmann, A.M. Braun, Lanthanide oxide doped titanium dioxide photocatalysts: effective photocatalysts for the enhanced degradation of salicylic acid and t-cinnamic acid, J. Catal. 204 (2001) 305–313.
[20] K.T. Ranjit, I. Willner, S.H. Bossmann, A.M. Braun, Lanthanide oxide-doped titanium dioxide photocatalysts: Novel photocatalysts for the enhanced degradation of p-chlorophenoxyacetic acid, Environ. Sci. Technol. 35 (2001) 1544–1549.
[21] F.B. Li, X.Z. Li, K.H. Ng, Photocatalytic degradation of an odorous pollutant: 2-mercaptobenzothiazole in aqueous suspension using Nd^{3+}–TiO_2 catalysts, Ind. Eng. Chem. Res. 45 (2006) 1–7.
[22] Y. Zhang, H. Zhang, Y. Xu, Y. Wang, Europium doped nanocrystalline titanium dioxide: preparation, phase transformation and photocatalytic properties, J. Mater. Chem. 13 (2003) 5.
[23] Y. Zhang, H. Zhang, Y. Xu, Y. Wang, Significant effect of lanthanide doping on the texture and properties of nanocrystalline mesoporous TiO_2, J. Solid State Chem. 177 (2004) 3490–3498.
[24] X.Z. Shen, Z.C. Liu, S.M. Xie, J. Guo, Degradation of nitrobenzene using titania photocatalyst co-doped with nitrogen and cerium under visible light illumination, J. Hazard. Mater. 162 (2009) 1193–1198.
[25] D.G. Huang, S.J. Liao, W.B. Zhou, S.Q. Quan, L. Liu, Z.J. He, J.B. Wan, Synthesis of samarium- and nitrogen-co-doped TiO_2 by modified hydrothermal method and its photocatalytic performance for the degradation of 4-chlorophenol, J. Phys. Chem. Solids 70 (2009) 853–859.
[26] X. Ding, X. Liu, Correlation between anatase-to-rutile transformation and grain growth in nanocrystalline titania powders, J. Mater. Res. 13 (1998) 2556–2559.
[27] E.L. Crepaldi, G.J.d.A.A. Soler-Illia, D. Grosso, F. Cagnol, F. Ribot, C. Sanchez, Controlled formation of highly organized mesoporous titania thin films: From mesostructured hybrids to mesoporous nanoanatase TiO_2, J. Am. Chem. Soc. 125 (2003) 9770–9786.
[28] R.A. Spurr, H. Myers, Quantitative analysis of anatase–rutile mixtures with an X-ray diffractometer, Anal. Chem. 29 (1957) 760–762.
[29] K. Tennakone, C. Thaminimulla, W. Kiridena, Nitrogen photoreduction by coprecipitated hydrous oxides of samarium(III) and vanadium(III), Langmuir 9 (1993) 723–726.
[30] X.B. Chen, C. Burda, Photoelectron spectroscopic investigation of nitrogen-doped titania nanoparticles, J. Phys. Chem. B 108 (2004) 15446–15449.
[31] L. Lin, R.Y. Zheng, J.L. Xie, Y.X. Zhu, Y.C. Xie, Synthesis and characterization of phosphor and nitrogen co-doped titania, Appl. Catal. B: Environ. 76 (2007) 196–202.
[32] N.C. Saha, H.G. Tompkins, Titanium nitride oxidation chemistry: an X-ray photoelectron spectroscopy study, J. Appl. Phys. 72 (1992) 3072–3079.
[33] J.W. Wang, W. Zhu, Y.Q. Zhang, S.X. Liu, An efficient two-step technique for nitrogen-doped titanium dioxide synthesizing: visible-light-induced photodecomposition of methylene blue, J. Phys. Chem. C 111 (2007) 1010–1014.
[34] M. Sathish, B. Viswanathan, R. Viswanath, C. Gopinath, Synthesis, characterization, electronic structure, and photocatalytic activity of nitrogen-doped TiO_2 nanocatalyst, Chem. Mater. 17 (2005) 6349–6353.
[35] C.H. Liang, F.B. Li, C.S. Liu, J.L. Lü, X.G. Wang, The enhancement of adsorption and photocatalytic activity of rare earth ions doped TiO_2 for the degradation of orange II, Dyes Pigments 76 (2008) 477–484.
[36] A.D. Weisz, L. Garcia Rodenas, P.J. Morando, A.E. Regazzoni, M.A. Blesa, FTIR study of the adsorption of single pollutants and mixtures of pollutants onto titanium dioxide in water: oxalic and salicylic acids, Catal. Today 76 (2002) 103–112.